Microchemical Journal 155 (2020) 104788

Contents lists available at ScienceDirect

Microchemical Journal

journal homepage: www.elsevier.com/locate/microc

Detection of zinc (II) and hypochlorite by a thiourea-based chemosensor via two emission channels and its application in vivo

Haeri So[a], Hanna Cho[a,*], Hangyul Lee[a], Minh Cong Tran[b], Ki-Tae Kim[b,*], Cheal Kim[a,*]

[a] Department of Fine Chem., Seoul National Univ. of Sci. and Tech. (SNUT), Seoul 01088, Korea
[b] Department of Chemistry, Seoul National Univ. of Sci. and Tech. (SNUT), Seoul 01188, Korea

ARTICLE INFO

Keywords:
Fluorometric analysis
Hypochlorite
Zinc ion
Zebrafish
Water sample
Theoretical calculations

ABSTRACT

A novel thiourea-based chemosensor **THB** (N-benzhydryl-2-(thiophene-2-carbonyl)hydrazine-1-carbothioamide) was designed and investigated. **THB** had the capability to detect zinc ion and hypochlorite in a near-perfect aqueous media via different fluorescent emission channels. Limits of detection (LOD) were determined to be 0.67 μM for zinc ion and 0.28 μM for hypochlorite. Importantly, **THB** could successfully monitor both zinc ion and hypochlorite in zebrafish. Response mechanisms of **THB** to zinc ion and hypochlorite were demonstrated by ^{1}H NMR titrations, theoretical calculations, fluorescent and UV–vis spectral variations, and ESI-mass.

1. Introduction

The research on chemosensors for detecting diverse metal ions and anions has attracted much attention due to their wide applicability in biological, pathological, and industry environments [1,2]. Among the various metal ions, zinc ion is the second plentiful metal element in the human body and plays critical roles in metabolism including enzymatic reactions, brain functioning, DNA organization, and gene expression [3,4]. However, the disorder of zinc metabolism adversely affects brain functioning, blood cholesterol level, hair, and skin health [5–7] and also causes neurogenic diseases like Alzheimer's disease [8,9]. Thus, it is greatly significant to design chemosensors for monitoring zinc.

Hypochlorite, as a potential oxidant in ROS (reactive oxygen species), is generally produced from the peroxidation reaction between H_2O_2 and Cl^- in living organisms with the assistance of myeloperoxidase [10–12]. Hypochlorite plays critical roles in the immune defense of pathogen invasion [13,14]. However, the uncontrolled generation of hypochlorite may induce many problems such as neurodegenerative disorders and damage of tissue and organ [15,16]. In addition, water containing residual Cl^- adversely affects the blood circulation and nervous system [17,18]. Thus, it is of significant interest to study chemosensor for recognizing hypochlorite in water.

Among the various analytical tools, fluorometric analysis is a significantly preferred optical tool due to their high selectivity, sensitivity, fast response, and especially the capability of bioimaging [19–21]. To date, a number of fluorescence chemosensors for monitoring zinc or hypochlorite have been reported [22–28] and some of them have the capability to monitor the analytes in *vitro* and in *vivo* [29–35]. However, any fluorescent chemosensor detecting both zinc ion and hypochlorite has not been reported yet.

Thiourea has drawn much interest due to its diverse biological properties and ability as a recognition group toward various analytes [5,36,37]. Because the thiourea contains nitrogen, oxygen and sulfur atoms acting as electron-donor atoms, it has an excellent chelating capability to metal ions [38–41] and could undergo oxidation reaction by ROS like ClO^- [42–44]. Therefore, we expected that a thiourea-based chemosensor could chelate metal ions and respond to ROS like hypochlorite by oxidation.

Herein, we developed a thiourea-based fluorescent chemosensor **THB** which could detect both zinc ion and hypochlorite. In addition, **THB** had a great capability to detect both zinc ion and hypochlorite in *vivo*. The response mechanisms of **THB** to zinc ion and hypochlorite were demonstrated, based on ^{1}H NMR titrations, theoretical calculations, fluorescent and UV–vis spectral variations, and ESI-mass.

2. Experiments

2.1. General information

All reagents were provided commercially. ^{1}H NMR and ^{13}C NMR were collected on a Varian spectrometer. Absorption and fluorescent spectra were collected on Perkin Elmer spectrometers. Quadrupole ion trap instrument was employed to get ESI-mass data. Agilent Cary 670 spectrometer was employed to obtain FT-IR spectra.

* Corresponding authors.
E-mail addresses: 1114chn@gmail.com (H. Cho), ktkim@snut.ac.kr (K.-T. Kim), chealkim@snut.ac.kr (C. Kim).

https://doi.org/10.1016/j.microc.2020.104788
Received 27 November 2019; Received in revised form 26 February 2020; Accepted 1 March 2020
Available online 03 March 2020
0026-265X/

2.2. Synthesis of N-benzhydryl-2-(thiophene-2-carbonyl)hydrazine-1-carbothioamide (THB)

Thiophene-2-carbohydrazide (0.17 g, 1.2 × 10^{-3} mol) was dissolved in 6 mL of ethanol and benzhydryl isothiocyanate (0.23 g, 1.0 × 10^{-3} mol) was added into the solution. With stirring for 1 d, white precipitation was formed, filtered, and washed with diethyl ether and ethanol (yield: 78%). MP (melting point): 113–118 °C. ^{1}H NMR (400 MHz, DMF-d_7), δ (ppm): 10.51 (s, 1H), 9.52 (s, 1H), 9.16 (s, 1H), 7.91 (m, 1H), 7.88 (d, J = 4.8 Hz, 1H), 7.35 (m, 7H), 7.29 (m, H), 7.21 (m, 1H), 7.14 (s, 1H). ^{13}C NMR (100 MHz, DMF-d_7), δ (ppm): 142.52 (1C), 138.50 (1C), 132.45 (2C), 130.33 (1C), 129.05 (2C), 128.90 (5C), 128.72 (4C), 127.86 (2C), 61.56 (1C). FT-IR (KBr) for **THB** (cm^{-1}): N−H (3367, 3308, 3203); $C = O$ (1656); $C = S$ (1526); C−N (1231). ESI-MS for $[\mathbf{THB}+H^+]^+$: found, 368.0097; $[C_{19}H_{17}N_3OS_2 + H^+]^+$ requires $[\mathbf{THB}+H^+]^+$ 368.0886.

2.3. Fluorescent and UV-visible spectral measurements

All fluorescence and UV-visible experiments were performed in PBS buffer (10 mM, pH 7.4). A **THB** stock (5 mM) was prepared in DMSO and the concentration of **THB** used in the experiments was 20 μM for zinc (II) and 10 μM for hypochlorite, respectively. All the cation and anion stocks were prepared in bis-tris buffer and ROS stocks were prepared in distilled water. Fluorescent and UV–vis spectral variations for zinc (II) and hypochlorite were measured by adding corresponding concentrations of the analytes to **THB** solution and mixing them for 10 s.

2.4. Quantum yields

The quantum yields of **THB** and **THB**-Zn^{2+}, **THB**-ClO^- were determined with quinine (Φ = 0.54 in 100 mM H_2SO_4 solution) as a reference fluorophore [45]. The quantum yields were calculated with the following equation [46].

$$\Phi_{FS} = \Phi_{FR} \times \frac{A_R \times F_S}{A_S \times F_R} \times \left(\frac{n_S}{n_R}\right)^2$$

Φ_F = fluorescence quantum yield
A = absorbance
F = integrated fluorescence emission
n = refractive index of the solution
S = test sample
R = reference material

2.5. ^{1}H NMR titrations

For zinc (II), the four NMR glass tubes of **THB** (4.9 mg, 2 × 10^{-5} mol) dissolved in DMF-d_7 (1.0 mL) were prepared. Various amounts (0, 0.5, 1, and 2 equiv) of zinc (II) were added into the NMR tubes of **THB**. After mixing them for 10 s, the ^{1}H NMR spectra were gained. For hypochlorite, the four NMR tubes of **THB** (4.9 mg, 0.02 mmol) dissolved in DMF-d_7 (1.0 mL) were prepared. Various amounts (0, 0.5, 2, and 5 equiv) of hypochlorite were transferred to the NMR tubes of **THB**, respectively. After mixing them for 10 s, the ^{1}H NMR spectra were gained.

2.6. Analysis of hypochlorite

The sample solutions were gained from the drinking water and tap water in our laboratory. 12 μL of **THB** stock (5 mM) and 0.30 mL of PBS buffer (1 × 10^{-2} M) were added into 2.688 mL sample solutions containing hypochlorite. After blending them for 10 s, fluorescence spectra were gained.

2.7. Imaging experiments in zebrafish

Zebrafish were cultured at 28.5 °C under previously reported conditions [47]. The 6-day-old zebrafish were prepared and three zebrafish groups were treated with **THB** (5 × 10^{-6} M) in E2 media having 0.05% DMSO for 20 min and then washed with E2 media to remove the remaining **THB**. Except for a control group, two groups were further treated with the solution containing 5 and 10 μM of Zn^{2+} for 20 min and then washed with E2 media to remove the remaining Zn^{2+}. Ethyl-3-aminobenzoate methanesulfonate was used for the secured orientation of zebrafish. The fluorescence images were acquired with a Leica fluorescence microscope and the mean intensity was determined by Icy software. The similar procedures were performed for hypochlorite.

2.8. Cytotoxicity in zebrafish

The cytotoxicity in zebrafish upon treatment with **THB** was measured by acridine orange (AO) staining. The 6-day-old zebrafish were prepared and exposed to 0 and 50 μM of **THB** in E2 media having 0.5% of DMSO for 20 min. These zebrafish were exposed to 10 μg/mL of AO reagent (Sigma-Aldrich, St. Louis, MO, USA) in E2 media for 60 min. After the zebrafish were washed with E2 media three times, the fluorescence images were acquired under a Leica fluorescence microscope (MZ10F, Singapore).

2.9. Theoretical studies

The sensing mechanism of **THB** to Zn^{2+} and ClO^- was studied by the calculation with Gaussian 09 software [48]. Geometric optimizations and DFT (density functional theory) calculations [49,50] were performed at the B3LYP/6–311 G/LANL2DZ level [51–55] and CPCM was employed to consider the effect of solvent water [56,57].

3. Results and discussion

THB was produced from the nucleophilic addition reaction of thiophene-2-carbohydrazide and benzhydryl isothiocyanate (Scheme 1) and verified by ESI-mass, FT-IR, ^{1}H NMR and ^{13}C NMR analysis (Fig. S1).

3.1. Fluorescent and UV-visible studies of THB to zinc (II)

To evaluate the sensing ability of **THB**, fluorescent response of **THB** to diverse metal ions was studied (Fig. 1). **THB** showed no fluorescence emission around 465 nm. Upon the addition of Zn^{2+}, **THB** showed a remarkable fluorescence emission at 465 nm with a sky-blue fluorescence color (10 mM PBS buffer pH 7.4; λ_{ex} = 345 nm, λ_{em} = 465 nm, Stokes shift = 120 nm, $t_{1/2}$ = 2 h). In contrast, the addition of other metals displayed no or small spectral variation. These results indicated

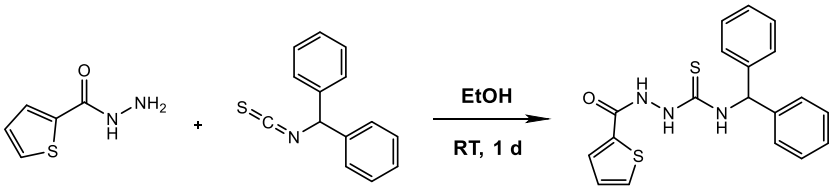

Scheme 1. Synthesis of **THB**.

that **THB** was capable of being a selective fluorescent chemosensor for Zn^{2+}.

The sensing phenomena of **THB** to Zn^{2+} were studied by the examination of fluorescent and UV-visible variations. Upon addition of Zn^{2+} (0–1.1 equiv), the fluorescence at 465 nm was consistently enhanced (Fig. 2). Quantum yields of **THB** and **THB**-Zn^{2+} turned out to be 0.0269 and 0.0704, respectively. Under the same condition, UV–vis spectral variations were studied (Fig. S2; λ_{max} = 322 nm, ε_{max} = 5775.42 mol^{-1} dm^3 cm^{-1}). A gradual increase of the absorbance at 322 nm and a decrease of the absorbance at 245 nm were observed with a definite isosbestic point at 256 nm. It meant the generation of a species between **THB** and Zn^{2+}.

Job plot was examined for understanding the mode of complexation between **THB** and Zn^{2+} (Fig. 3). The highest emission at 465 nm was shown at a mole fraction of 0.7, indicating a 2 to 1 ratio of **THB** and Zn^{2+}. It was supported by ESI-mass (Fig. S3). The peak of 797.0071 (*m/z*) corresponded to [2•**THB**-H^+ + Zn^{2+}]$^+$ (calcd; 797.0834). With the fluorescence data, the detection limit for Zn^{2+} was calculated to be 0.67 μM by using the definition of IUPAC (C_{DL} = 3σ/K) [58], which is far lower than WHO protocol (76 μM) (Fig. S4). [59]. The association constant of **THB** with Zn^{2+} was gained to be 2 × 10^{10} M^{-2} (R^2 = 0.9903) based on Li's equation (Fig. S5).

^{1}H NMR titrations were conducted to understand the complexation of **THB** to Zn^{2+} (Fig. S6). Upon the addition of Zn^{2+} of 0.5 equiv, most proton peaks showed down-field shifts. With the more addition of Zn^{2+} up to 2 equiv, the integration of -NH (H_4 and $H_{4'}$) reduced to half, meaning deprotonation of one H_4 of 2•**THB** by binding to Zn^{2+}. These results demonstrated that the sulfur atoms and -NH were highly associated with the binding to Zn^{2+}. We proposed the response mechanism of **THB** to Zn^{2+}, based on Job plot, ESI-mass, and ^{1}H NMR titrations (Scheme 2).

Competition experiment was performed to study a sensing capability of **THB** to Zn^{2+} (Fig. S7). Most metal ions didn't show inhibition in the fluorescence emission of **THB** to Zn^{2+}. However, the presence of Fe^{2+}, Hg^{2+}, and Co^{2+} showed the inhibition of 10 to 50%, and Cu^{2+} and Cr^{3+} nearly inhibited. The pH test of **THB** to Zn^{2+} was examined at the pH range of 6 to 8 (Fig. S8). The addition of Zn^{2+} induced the enhancement of fluorescence emission of **THB** at the pH range of 7 and 8, suggesting that **THB** does not operate as a Zn^{2+} sensor under the acidic condition. The sulfur atom of **THB** might be protonated under the acidic condition. Therefore, it is difficult for Zn^{2+} to bind to the protonated sulfur atom.

3.2. Fluorescence and UV–vis studies of *THB* to hypochlorite

Fluorescent response of **THB** to various anions and ROS was studied (Fig. 4). In the presence of ClO^-, **THB** showed marked fluorescence emission at 380 nm with deep blue fluorescence color (10 mM PBS buffer pH 7.4; λ_{ex} = 300 nm, λ_{em} = 380 nm, Stokes shift = 80 nm). By contrast, no spectral variation was observed with other anions and ROS, demonstrating that **THB** could be a highly selective fluorescent chemosensor for hypochlorite.

The sensing properties of **THB** to ClO^- were explored by fluorescent and UV–vis spectral variations. With the addition of ClO^- (0–14 equiv), continuous enhancement of the fluorescence emission band at 380 nm was observed (Fig. 5). Quantum yields of **THB** and **THB**-ClO^- were determined to be 0.0132 and 0.9192, respectively. Under the same condition, UV–vis spectral variations were inspected (Fig. S9; λ_{max} = 298 nm, ε_{max} = 1155.83 mol^{-1} dm^3 cm^{-1}). The gradual addition of ClO^- induced a marked increase of the absorbance at 300 nm and a decrease at 240 nm with a clear isosbestic point at 277 nm. It meant the production of a species between **THB** and ClO^-.

^{1}H NMR titrations were conducted to understand the response reaction of **THB** to ClO^- (Fig. S10). Upon the addition of ClO^- up to 5 equiv, the protons H_4, H_5, and H_6 gradually disappeared and the rest protons showed up-field shifts, meaning deprotonation of the -NH groups by ClO^-. To further understand these phenomena, negative ESI-MS was carried out (Fig. S11). The peak of *m/z* 366.2500 was found and corresponded to [$C_{19}H_{14}N_3O_2S^-$ + H_2O]$^-$ (calcd; 366.0912), indicating the deprotonation of the -NH groups and the oxidation of the thionyl moiety to the carbonyl one by ClO^-. These results led us to conclude that **THB** responded to ClO^- through the deprotonation and oxidation reaction (Scheme 3).

Competition test was examined to explore a sensing capability of **THB** to hypochlorite (Fig. 6). The presence of diverse anions and ROS showed no or a neglectable inhibition in the fluorescence emission, implying that the sensing capability of **THB** to ClO^- was not nearly affected by other analytes. The pH test of **THB** to ClO^- was performed at the pH range of 6 to 8 (Fig. S12). With the addition of ClO^-, **THB** showed the clear enhancement of fluorescence emission at the pH range of 7 and 8, suggesting that **THB** does not operate as a ClO^- sensor under the acidic condition. That is, HClO species produced from the binding of H^+ and ClO^- under the acidic condition is not competent to the deprotonation and oxidation of **THB**.

To explore the quantitative sensing capability of **THB**, a calibration plot was obtained with a satisfactory linearity (R^2 = 0.9996) (Fig. S13). On the basis of this plot, the detection limit turned out to be 0.28 μM by using the definition of IUPAC (C_{DL} = 3σ/k) [58]. The potential applicability of **THB** toward ClO^- was tested in real samples (Table 1). In both tap water and drinking water, suitable recoveries and R.S.D. values were obtained, implying that **THB** has great applicability for detecting ClO^- in real samples.

3.3. Bioimaging application in zebrafish

To study the bioimaging applications of **THB** to $Zn^{2+}$and ClO^-, fluorescent imaging experiments were performed in zebrafish (Figs. 7 and 8). The zebrafish treated with **THB** showed negligible fluorescence emission in the green channel. With the further treatment of Zn^{2+} (5 and 10 μM), the strengthened fluorescence emission was shown in the swim bladder and eyes of zebrafish. In the swim bladder, the mean fluorescence intensity and detection limit (4.63 μM) were obtained by using icy software (Fig. S14). Under the same condition, the further treatment of ClO^- (5 and 10 μM) induced strengthened fluorescence emission in the tail and swim bladder of zebrafish. The mean fluorescence intensity was obtained in tail and detection limit was gained to be

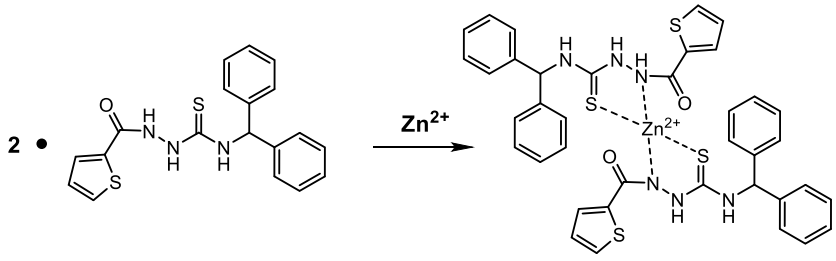

Scheme 2. Response mechanism of **THB** to zinc ion.

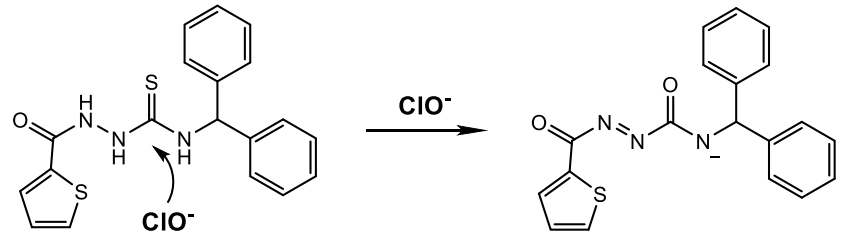

Scheme 3. Response mechanism of **THB** to hypochlorite.

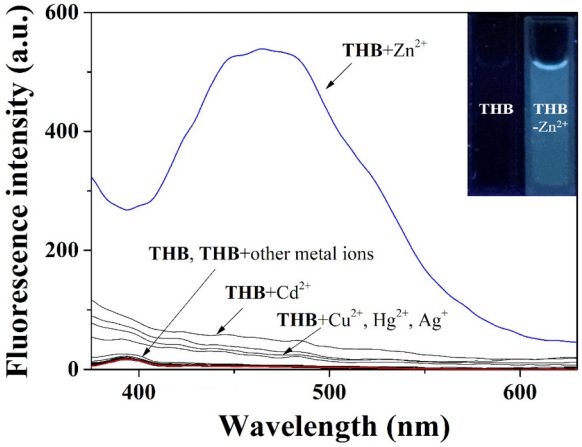

Fig. 1. Fluorescence response of **THB** toward diverse metal ions. Inset: Fluorescent image of **THB** and **THB**-Zn^{2+}.

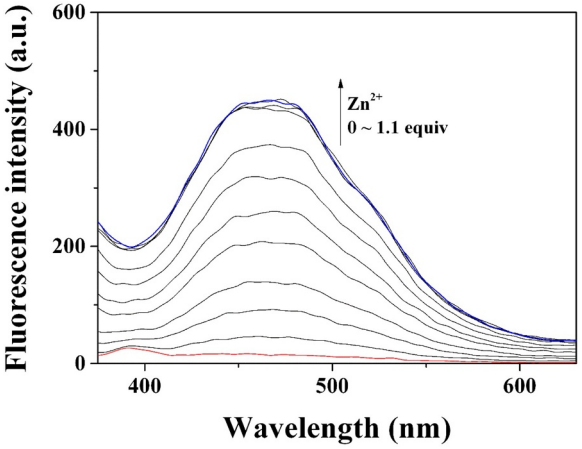

Fig. 2. Fluorescence spectral variations of **THB** (20 uM) in the presence of different concentrations of Zn^{2+}.

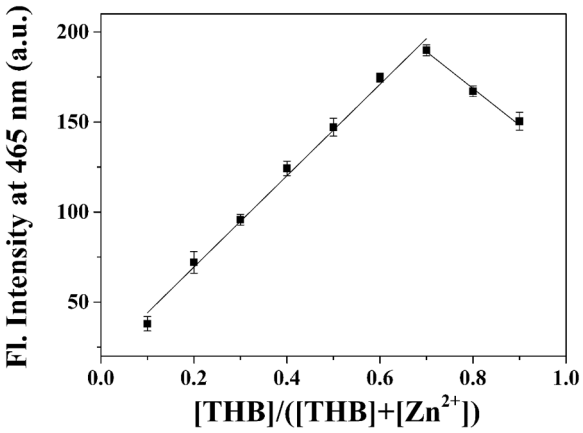

Fig. 3. Job plot analysis of **THB** with Zn^{2+} (20 μM).

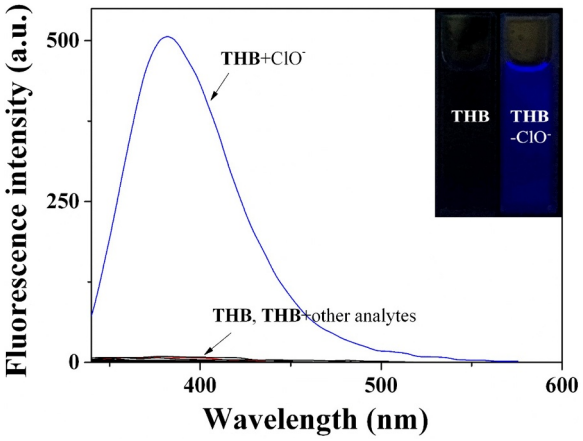

Fig. 4. Fluorescence response of **THB** toward diverse analytes. Inset: Fluorescent image of **THB** and **THB**-ClO^-.

0.51 μM (Fig. S15). The cytotoxicity study was examined by AO staining. As shown in Fig. S16, there is no difference in bright spots of two AO-stained groups of zebrafish. These results implied that **THB** with no toxicity could be applied to fluorescent imaging of both Zn^{2+} and ClO^- in *vivo*.

3.4. Theoretical studies

^{1}H NMR titrations and ESI-mass results led us to optimize possible structures of **THB,** **THB**-Zn^{2+} and **THB**-ClO^-. Optimized structures are shown in Fig. 9. **THB** having a twisted structure had a dihedral angle close to the right angle (1C, 2 N, 3 N, 4C = −99.002° and 5S, 6 N, 7 N, 8O = −81.091°). The optimized **THB**-Zn^{2+} showed that both the nitrogen and sulfur atoms in **THB** were used as binding sites to zinc ion (1C, 2 N, 3 N, 4C = 171.805°). In the case of **THB**-ClO^-, the substitution of the sulfur atom in thiourea moiety to oxygen atom and the deprotonation of H_4, H_5, and H_6 generated a double bond between two nitrogen atoms. The investigation of possible twenty transition states was proceeded by TD-DFT, a cost-effective tool for calculating the electronic transitions of molecules. The molecular orbitals were analyzed, on the basis of the major transition state well matched with the experimental results. The major transitions of **THB** at 254.52 nm stemmed from HOMO-6 and HOMO-3 to LUMO transitions, and their characteristics consisted of dominant π-π* transition in the thiophene and small portion of ICT (intramolecular charge transfer) from the diphenylmethane to the thiophene moiety (Figs. S17 and S18). Similar to **THB**, the charge transfer character of **THB**-Zn^{2+} at 305.85 nm was dominated by π-π* transition and ICT character as well (HOMO-2→LUMO and HOMO→LUMO+1) (Figs. S18 and S19). Given that the transition characters of **THB** and **THB**-Zn^{2+} were analogous and the angle of the **THB** in the complex has become more rigid, the fluorescence turn-on mechanism for **THB**-Zn^{2+} would be CHEF (chelation-

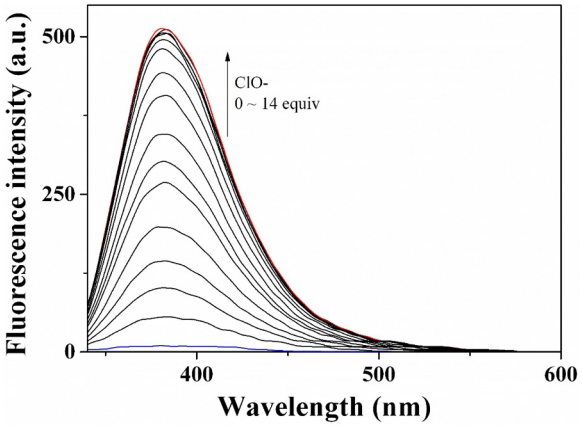

Fig. 5. Fluorescence spectral variations of **THB** (10 uM) in the presence of different concentrations of ClO^-.

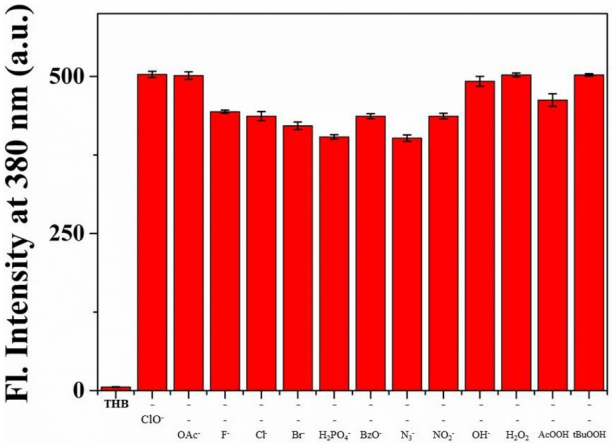

Fig. 6. Fluorescence intensity (380 nm) of **THB** toward ClO^- in the presence of diverse analytes.

Table 1
Analysis of ClO^-.[a].

Sample	ClO^- added (μM)	ClO^- found (μM)	Recovery (%)	R.S.D (n = 3) (%)
Tap water	0.00	0.00	–	–
	5.00	4.97	99.33	1.57
Drinking water	0.00	0.00	–	–
	5.00	5.07	101.44	0.79

[a] Conditions: [**THB**] = 10 μM in PBS buffer (pH = 7.4, 10 mM).

enhanced fluorescence) effect [46]. Non-radiative transitions, such as vibrations and rotations, presented in **THB** might be inhibited and converted to radiative transition by chelation with Zn^{2+}.

Substituted from the sulfur atom to oxygen atom in **THB,** **THB**-ClO^- exhibited the main absorption at 277.60 nm which consisted of HOMO-8 → LUMO and HOMO-7 → LUMO transitions (Figs. S20 and S21). In the transition states, only π-π* transition character near the thiophene moiety was observed. Therefore, the elimination of protons and the oxidation of the thionyl to the carbonyl moiety by ClO^- resulted in blocking ICT process from the diphenylmethane to the thiophene. The inhibition of ICT, non-radiative process, would induce radiative transition, especially fluorescence emission [60]. To sum up, we proposed the plausible sensing mechanisms of Zn^{2+} and ClO^- by **THB**, based on experimental and theoretical results (Schemes 2 and 3).

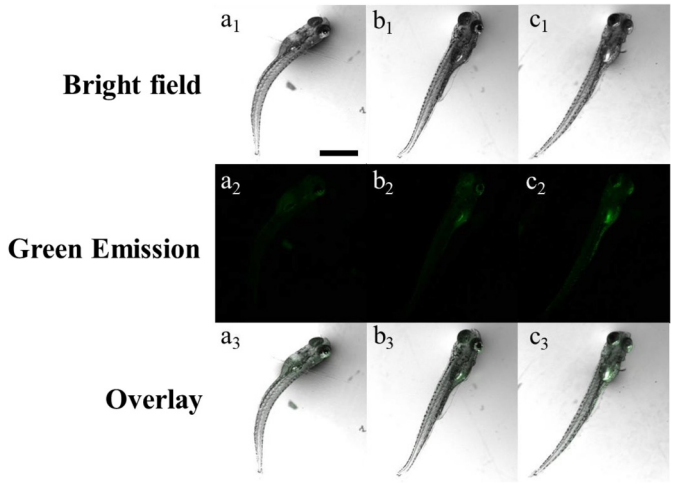

Fig. 7. Fluorescence images of zebrafish (6-day-old) treated with **THB**, followed by addition of Zn^{2+}. (a_1-a_3): **THB** only; (b_1-b_3): **THB** with 5 μM Zn^{2+}; (c_1-c_3): **THB** with 10 μM Zn^{2+}. [**THB**] = 5 μM. Scale bar: 1.03 mm.

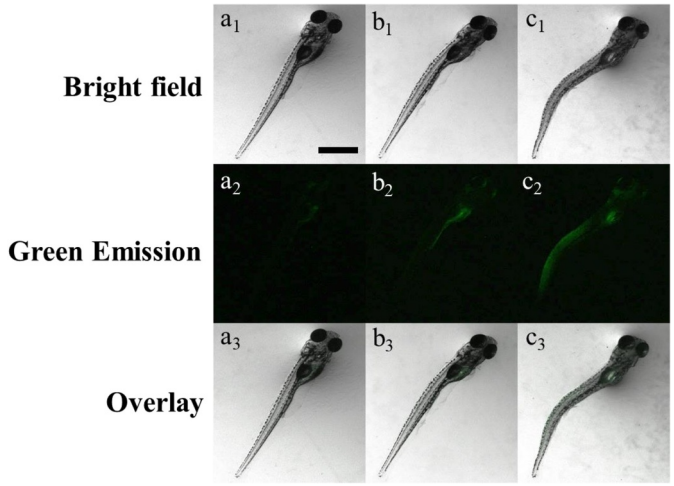

Fig. 8. Fluorescence images of zebrafish (6-day-old) treated with **THB**, followed by addition of ClO^-. (a_1-a_3): **THB** only; (b_1-b_3): **THB** with 5 μM ClO^-; (c_1-c_3): **THB** with 10 μM ClO^-. [**THB**] = 5 μM. Scale bar: 1.03 mm.

4. Conclusion

A new bifunctional fluorescent turn-on chemosensor **THB** was developed. **THB** could detect both zinc ion and hypochlorite for the first time, showing obvious fluorescence emissions. The detection limits of zinc ion and hypochlorite turned out to be 0.67 μM and 0.28 μM, which were lower than WHO protocols. In addition, **THB** showed the quantitative sensing ability for hypochlorite in real samples. Particularly, **THB** could be applied as a bioimaging fluorescent chemosensor for both Zn^{2+} and hypochlorite in *vivo*. The response mechanisms to zinc ion and hypochlorite were demonstrated by various spectroscopic outcomes and theoretical calculations.

CRediT authorship contribution statement

Haeri So: Investigation, Validation. **Hanna Cho:** Investigation, Validation. **Hangyul Lee:** Software, Formal analysis. **Minh Cong Tran:** Investigation, Validation. **Ki-Tae Kim:** Writing - review & editing, Supervision. **Cheal Kim:** Writing - review & editing, Supervision.

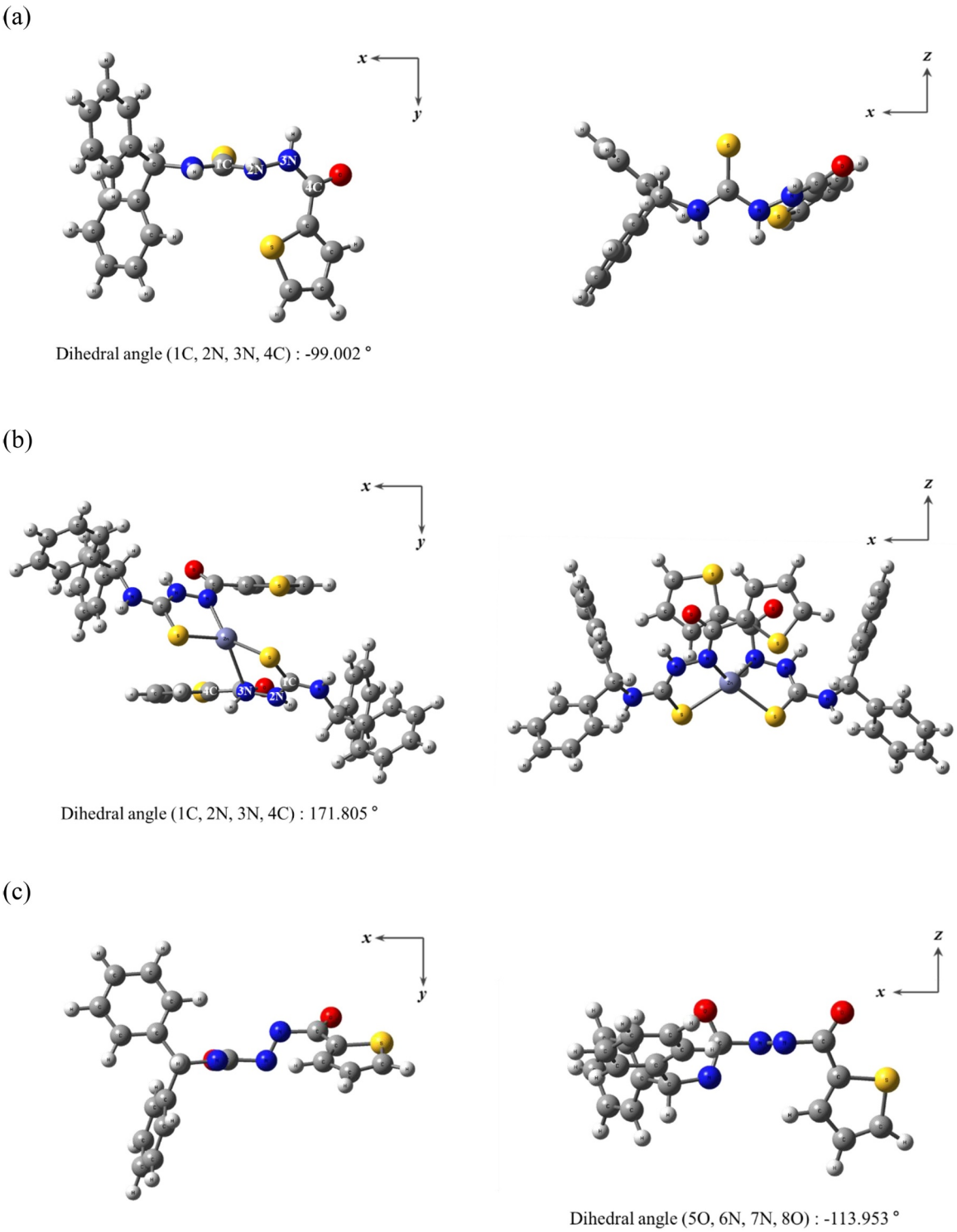

Fig. 9. Energy-optimized structures of (a) **THB**, (b) **THB**-Zn^{2+} and (c) **THB**-ClO^{-}.

Declaration of Competing Interest

The authors declare that they have no known competing financial interests or personal relationships that could have appeared to influence the work reported in this paper.

Acknowledgments

This work was supported by Korea Environment Industry & Technology Institute (KEITI) through ``The Chemical Accident Prevention Technology Development Project", funded by Korea Ministry of Environment (MOE) (No. 2016001970001) and National Research Foundation of Korea (2018R1A2B6001686).

Supplementary materials

Supplementary material associated with this article can be found, in the online version, at doi:10.1016/j.microc.2020.104788.

References

[1] D. Maity, D. Karthigeyan, T.K. Kundu, T. Govindaraju, FRET-based rational strategy for ratiometric detection of Cu^{2+} and live cell imaging, Sens. Actuators B. 176 (2013) 831–837.

[2] X.Q. Ma, Y. Wang, T.B. Wei, L.H. Qi, X.M. Jiang, J.D. Ding, W.B. Zhu, H. Yao, Y.M. Zhang, Q. Lin, A novel AIE chemosensor based on quinoline functionalized pillar[5]arene for highly selective and sensitive sequential detection of toxic Hg^{2+} and CN^-, Dyes Pigm. 164 (2019) 279–286.

[3] S.Y. Lee, S.Y. Kim, J.A. Kim, C. Kim, A dual chemosensor: colorimetric detection of Co^{2+} and fluorometric detection of Zn^{2+}, J. Lumin. 179 (2016) 602–609.

[4] K. Jiang, S. Chen, S. Luo, C. Pang, X. Wu, Z. Wang, Concise synthesis of water soluble fluorescence sensor for sequential detection of Zn (II) and picric acid via cascade mechanism, Dyes Pigm. 167 (2019) 164–173.

[5] B. Hu, B. Wang, B. Zhao, Q. Guo, Z.H. Li, X.H. Zhang, G.Y. Liu, Y. Liu, Y. Tang, F. Luo, Y. Du, Y.X. Chen, L.Y. Ma, H.M. Liu, Thiosemicarbazone-based selective proliferation inactivators inhibit gastric cancer cell growth, invasion, and migration, Medchemcomm 8 (2017) 2173–2180.

[6] N. Narayanaswamy, D. Maity, T. Govindaraju, Reversible fluorescence sensing of Zn^{2+} based on pyridine-constrained bis(triazole-linked hydroxyquinoline) sensor, Supramol. Chem. 23 (2011) 703–709.

[7] A. Pandith, N. Uddin, C.H. Choi, H.-.S. Kim, Highly selective imidazole-appended 9,10-N,N″-diaminomethylanthracene fluorescent probe for switch-on Zn^{2+} detection and switch-off $H_2PO_4^-$ and CN^- detection in 80% aqueous DMSO, and applications to se, Sens. Actuators B. 247 (2017) 840–849.

[8] D. Liu, X. Yin, X. Deng, J. Shi, H. Zhu, Z. Shang, J. Chen, G. Yang, H. He, 1, 8-Naphthalimide-based fluorescent sensor with highly selective and sensitive detection of Zn^{2+} in aqueous solution and living cells, Inorg. Chem. Commun. 106 (2019) 43–47.

[9] V. Venkatesan, S. Kumar R, S.K.A. Kumar, S.K. Sahoo, Highly selective turn-on fluorogenic chemosensor for Zn^{2+} based on chelation enhanced fluorescence, Inorg. Chem. Commun. 102 (2019) 171–179.

[10] P. Sun, X. Chao, K. Wang, Z. Mao, Z. Liu, D. Cao, A coumarin Schiff's base two-photon fluorescent probe for hypochlorite in living cells and zebrafish, RSC Adv. 8 (2018) 6904–6909.

[11] Y.M. Zhang, J.X. He, W. Zhu, Y.F. Li, H. Fang, H. Yao, T.B. Wei, Q. Lin, Novel pillar [5]arene-based supramolecular organic framework gel for ultrasensitive response Fe^{3+} and F^- in water, Mater. Sci. Eng. C. 100 (2019) 62–69.

[12] J.-.T. Hou, H.S. Kim, C. Duan, M.S. Ji, S. Wang, L. Zeng, W. Ren, J.S. Kim, A ratiometric fluorescent probe for detecting hypochlorite in endoplasmic reticulum, Chem. Commun. (2019) 2533–2536.

[13] X. Xie, T. Wu, X. Wang, Y. Li, K. Wang, Z. Zhao, X. Jiao, B. Tang, A two-photon fluorescent probe for ratiometric visualization of hypochlorous acid in live cells and animals based on a selenide oxidation/elimination tandem reaction, Chem. Commun. 54 (2018) 11965–11968.

[14] H. Zhu, Z. Zhuang, B. Du, B. Zhu, Z. Li, P. Jia, B. Kang, W. Sheng, Q. Duan, C. Liu, Z. Wang, A highly specific and ultrasensitive p-aminophenylether-based fluorescent probe for imaging native HOCl in live cells and zebrafish, Anal. Chim. Acta. 1052 (2018) 131–136.

[15] L. Ni, Y. Wang, C. Li, J. Han, L. Ren, Y. Li, X. Bao, L. Wang, A water-soluble fluorescent probe for monitoring hypochlorite in water and in living cells, Sens. Actuators B. 273 (2018) 778–783.

[16] S. Goswami, K. Aich, S. Das, B. Pakhira, K. Ghoshal, C.K. Quah, M. Bhattacharyya, H.K. Fun, S. Sarkar, A triphenyl amine-based solvatofluorochromic dye for the selective and ratiometric sensing of OCl^- in human blood cells, Chem. - An Asian J. 10 (2015) 694–700.

[17] F. Qin, Y. Zhang, J. Zhu, Y. Li, W. Cao, Y. Ye, A mitochondrial-targeted fluorescent probe to sense pH and HOCl in living cells, Sens. Actuators B. 291 (2019) 207–215.

[18] R. Shi, H. Chen, Y. Qi, W. Huang, G. Yin, R. Wang, From aggregation-induced to solution emission: a new strategy for designing ratiometric fluorescent probes and its application for in vivo HCLO detection, Analyst 144 (2019) 1696–1703.

[19] J.-.H. Choi, A. Pandith, D. Chakradhar, H.-.R. Kim, H.-.S. Kim, Al^{3+}-Morpholine-appended Anthracene ensemble as a dual photonic switch for $H_2PO_4^-$ and CN^- ions and its biological applications, Bull. Korean Chem. Soc. 40 (2019) 138–145.

[20] L. Chen, S.J. Park, D. Wu, H.M. Kim, J. Yoon, A two-photon fluorescent probe for colorimetric and ratiometric monitoring of mercury in live cells and tissues, Chem. Commun. 55 (2019) 1766–1769.

[21] D.Y. Lee, N. Singh, D.O. Jang, A benzimidazole-based single molecular multianalyte fluorescent probe for the simultaneous analysis of Cu^{2+} and Fe^{3+}, Tetrahedron Lett 51 (2010) 1103–1106.

[22] B. Das, A. Jana, A. Das Mahapatra, D. Chattopadhyay, A. Dhara, S. Mabhai, S. Dey, Fluorescein derived Schiff base as fluorimetric zinc (II) sensor via 'turn on' response and its application in live cell imaging, Spectrochim. Acta A. 212 (2019) 222–231.

[23] S. Goswami, S. Maity, A.C. Maity, A.K. Das, Fluorometric and naked-eye detectable dual signaling chemodosimeter for hypochlorite, Sens. Actuators B. 204 (2014) 741–745.

[24] J. Liu, Z. Yin, A novel NIR-emissive probe with large stokes shift for hypochlorite detection and imaging in living cells, Talanta 196 (2019) 352–356.

[25] M. Shangguan, X. Jiang, Z. Lu, W. Zou, Y. Chen, P. Xu, Y. Pan, L. Hou, A coumarin-based fluorescent probe for hypochlorite ion detection in environmental water samples and living cells, Talanta 202 (2019) 303–307.

[26] Y.H. Yan, X.Y. He, L. Su, J.Y. Miao, B.X. Zhao, A new FRET-based ratiometric fluorescence probe for hypochlorous acid and its imaging in living cells, Talanta 201 (2019) 330–334.

[27] A. Pandey, S.K. Asthana, A. Prakash, J.K. Roy, I. Tiwari, K.K. Upadhyay, A selective hydrolytic and restructuring approach through a Schiff base design on a coumarin platform for "turn-on" fluorogenic sensing of Zn^{2+}, Dalton Trans. 48 (2019) 2068–2076.

[28] M.E. Shirbhate, Y. Jeong, G. Ko, G. Baek, G. Kim, Y.U. Kwon, K.M. Kim, J. Yoon, Selective fluorescent recognition of Zn^{2+} by using chiral binaphthol-pyrene probes, Dyes Pigm. 167 (2019) 29–35.

[29] Y. Zuo, Y. Zhang, B. Dong, Z. Gou, T. Yang, W. Lin, Binding reaction sites to polysiloxanes: unique fluorescent probe for reversible detection of CLO^-/GSH pair and the in situ imaging in live cells and zebrafish, Anal. Chem. 91 (2019) 1719–1723.

[30] P. Jia, Z. Zhuang, C. Liu, Z. Wang, Q. Duan, Z. Li, H. Zhu, B. Du, B. Zhu, W. Sheng, B. Kang, A highly specific and ultrasensitive p-aminophenylether-based fluorescent probe for imaging native HOCl in live cells and zebrafish, Anal. Chim. Acta. 1052 (2019) 131–136.

[31] T. Sarkar, S. Banerjee, A. Hussain, Significant photocytotoxic effect of an iron(iii) complex of a Schiff base ligand derived from vitamin B_6 and thiosemicarbazide in visible light, RSC Adv. 5 (2015) 29276–29284.

[32] P. Xing, Z. Zhang, Y. Niu, Y. Qi, L. Dong, C. Wang, Water solubility is essential for fluorescent probes to image hypochlorous acid in live cells, Chem. Commun. 54 (2018) 9889–9892.

[33] C. Liu, P. Jia, L. Wu, Z. Li, H. Zhu, Z. Wang, D. Shuo, W. Shu, X. Zhang, Y. Yu, B. Zhu, Rational design of a highly efficient two-photon fluorescent probe for tracking intracellular basal hypochlorous acid and its applications in identifying tumor cells and tissues, Sens. Actuators B. (2019) 126731.

[34] H. Song, Z. Zhang, A quinoline-based ratiometric fluorescent probe for discriminative detection of Zn^{2+} and Cd^{2+} with different binding modes, and its Zn^{2+} complex for relay sensing of pyrophosphate and adenosine triphosphate, Dyes Pigm. 165 (2019) 172–181.

[35] S.M. Hwang, D. Yun, H. Lee, M. Kim, M.H. Lim, K.T. Kim, C. Kim, Relay detection of Zn^{2+} and S^{2-} by a quinoline-based fluorescent chemosensor in aqueous media and zebrafish, Dyes Pigm. 165 (2019) 264–272.

[36] Y. Wang, Z. Wang, H. Kuang, Y. Zhang, W. Gu, Y. Zhu, S. Wang, Synthesis and antitumor activity of 2-isocamphanyl thiosemicarbazone derivatives via ROS-enhanced mitochondrial damage, Chem. Biol. Drug Des. 50 (2007) 3716–3729.

[37] D.S. Kalinowski, Y. Yu, P.C. Sharpe, M. Islam, Y.T. Liao, D.B. Lovejoy, N. Kumar, P.V. Bernhardt, D.R. Richardson, Design, synthesis, and characterization of novel iron chelators: structure-activity relationships of the 2-benzoylpyridine thiosemicarbazone series and their 3-nitrobenzoyl analogues as potent antitumor agents, J. Med. Chem. 50 (2007) 3716–3729.

[38] Z.E. Chen, H. Zhang, Z. Iqbal, A new thiosemicarbazone fluorescent probe based on 9,9′-bianthracene for Hg^{2+} and Ag^+, Spectrochim. Acta A. 215 (2019) 34–40.

[39] Z. Zhang, S. Lu, C. Sha, D. Xu, A single thiourea-appended 1,8-naphthalimide chemosensor for three heavy metal ions: Fe^{3+}, Pb^{2+}, and Hg^{2+}, Sens. Actuators B. 208 (2015) 258–266.

[40] S. Angupillai, J.Y. Hwang, J.Y. Lee, B.A. Rao, Y.A. Son, Efficient rhodamine-thiosemicarbazide-based colorimetric/fluorescent "turn-on" chemodosimeters for the detection of Hg^{2+} in aqueous samples, Sens. Actuators B. 214 (2015) 101–110.

[41] D. Udhayakumari, S. Suganya, S. Velmathi, Thiosemicabazone based fluorescent chemosensor for transition metal ions in aqueous medium, J. Lumin. 141 (2013) 48–52.

[42] A. Wibowo, J.M. Park, S.C. Liu, C. Khosla, D.M. Spielman, Real-Time in vivo detection of H_2O_2 using hyperpolarized ^{13}C-Thiourea, ACS Chem. Biol 12 (2017) 1737–1742.

[43] B. Shen, Y. Qian, Z. Qi, C. Lu, Q. Sun, X. Xia, Y. Cui, Near-infrared BODIPY-based two-photon CLO^- probe based on thiosemicarbazide desulfurization reaction: naked-eye detection and mitochondrial imaging, J. Mater. Chem. B. 5 (2017) 5854–5861.

[44] Z. Ma, X. Wang, C. Wang, X. Chen, Q. Lv, A sensitive and selective fluorescence probe for detection of hypochlorite (OCl^-) and its bioimaging in live cells, Spectrochim. Acta A. 213 (2019) 370–374.

[45] X. Li, Y. Sun, J. Chen, Z. Wu, P. Cheng, Q. Li, J. Fang, D. Chen, Enhanced fluorescence quantum yield of syndiotactic side-chain TPE polymers *via* RH-catalyzed carbene polymerization: influence of the substitution density and spacer length, Polym. Chem. 10 (2019) 1575–1584.

[46] C. Kim, J.B. Chae, A highly selective fluorescent chemosensor for detecting indium (III) with a low detection limit and its application, J. Fluoresc. 28 (2018) 1363–1370.

[47] G.J. Park, H. Kim, J.J. Lee, Y.S. Kim, S.Y. Lee, S. Lee, I. Noh, C. Kim, A highly selective turn-on chemosensor capable of monitoring Zn^{2+} concentrations in living cells and aqueous solution, Sens. Actuators B. 215 (2015) 568–576.

[48] M.J. Frisch, G.W. Trucks, H.B. Schlegel, G.E. Scuseria, M.A. Robb, J.R. Cheeseman, G. Scalmani, V. Barone, B. Mennucci, G.A. Petersson, H. Nakatsuji, M. Caricato, X. Li, H.P. Hratchian, A.F. Izmaylov, J. Bloino, G. Zheng, J.L. Sonnenberg, M. Hada, M. Ehara, K. Toyota, R. Fukuda, J. Hasegawa, M. Ishida, T. Nakajima, Y. Honda, O. Kitao, H. Nakai, T. Vreven, J.A. Montgomery, Jr., J.E. Peralta, F. Ogliaro, M. Bearpark, J.J. Heyd, E. Brothers, K.N. Kudin, V.N. Staroverov, R. Kobayashi, J. Normand, K. Raghavachari, A. Rendell, J.C. Burant, S.S. Iyengar, J. Tomasi, M. Cossi, N. Rega, J.M. Millam, M. Klene, J.E. Knox, J.B. Cross, V. Bakken, C. Adamo, J. Jaramillo, R. Gomperts, R.E. Stratmann, O. Yazyev, A.J. Austin, R. Cammi, C. Pomelli, J.W. Ochterski, R.L. Martin, K. Morokuma, V.G. Zakrzewski, G.A. Voth, P. Salvador, J.J. Dannenberg, S. Dapprich, A.D. Daniels, O. Farkas, J.B. Foresman, J.V. Ortiz, J. Cioslowski, and D.J. Fox, Gaussian 09 (Gaussian, Inc., Wallingford CT, 2009).

[49] A.D. Becke, Density-functional thermochemistry. III. the role of exact exchange, J. Chem. Phys. 98 (1993) 5648–5652.

[50] C. Lee, W. Yang, R.G. Parr, Development of the Colle-Salvetti correlation-energy

formula into a functional of the electron density, Phys. Rev. B. 37 (1988) 785–789.
[51] P.C. Hariharan, J.A. Pople, The influence of polarization functions on molecular orbital hydrogenation energies, Theor. Chim. Acta. 28 (1973) 213–222.
[52] M.M. Francl, W.J. Pietro, W.J. Hehre, J.S. Binkley, M.S. Gordon, D.J. DeFrees, J.A. Pople, Self-consistent molecular orbital methods. XXIII. a polarization-type basis set for second-row elements, J. Chem. Phys. 77 (1982) 3654–3665.
[53] P.J. Hay, W.R. Wadt, Ab initio effective core potentials for molecular calculations. potentials for the transition metal atoms *Sc* to Hg, J. Chem. Phys. 82 (1985) 270–283.
[54] W.R. Wadt, P.J. Hay, Ab initio effective core potentials for molecular calculations. potentials for main group elements Na to Bi, J. Chem. Phys. 82 (1985) 284–298.
[55] P.J. Hay, W.R. Wadt, *Ab initio* effective core potentials for molecular calculations. potentials for K to Au including the outermost core orbitals, J. Chem. Phys. 82 (1985) 299–310.
[56] V. Barone, M. Cossi, Quantum calculation of molecular energies and energy gradients in solution by a conductor solvent model, J. Phys. Chem. A. 102 (1998) 1995–2001.
[57] M. Cossi, V. Barone, Time-dependent density functional theory for molecules in liquid solutions, J. Chem. Phys. 115 (2001) 4708–4717.
[58] H. Kaur, N. Singh, N. Kaur, D.O. Jang, Nano-aggregate-Fe^{3+} complex based on benzimidazole-modified calix[4]arene for amplified fluorescence detection of ADP in aqueous media, Sens. Actuators B. 284 (2019) 193–201.
[59] World Health Organization, WHO Guidelines For Drinking-Water Quality -, 2nd edition, (1998) Volume 1, Geneva.
[60] H.J. Kim, K.C. Ko, J.H. Lee, J.Y. Lee, J.S. Kim, KCN sensor: unique chromogenic and 'turn-on' fluorescent chemodosimeter: rapid response and high selectivity, Chem. Commun. 47 (2011) 2886.